remote sensing

MDPI

Article

Intraspecific Differences in Spectral Reflectance Curves as Indicators of Reduced Vitality in High-Arctic Plants

Bogdan Zagajewski [1,*], Hans Tømmervik [2], Jarle W. Bjerke [2], Edwin Raczko [1], Zbigniew Bochenek [3], Andrzej Kłos [4], Anna Jarocińska [1], Samantha Lavender [5] and Dariusz Ziółkowski [3]

1 Department of Geoinformatics, Cartography and Remote Sensing, University of Warsaw (UW), ul. Krakowskie Przedmieście 30, 00-927 Warsaw, Poland; edwin.raczko@uw.edu.pl (E.R.); ajarocinska@uw.edu.pl (A.J.)
2 Norwegian Institute for Nature Research (NINA), FRAM—High North Research Centre for Climate and the Environment, P.O. Box 6606 Langnes, NO-9296 Tromsø, Norway; Hans.Tommervik@nina.no (H.T.); jarle.werner.bjerke@nina.no (J.W.B.)
3 Institute of Geodesy and Cartography (IGiK), ul. Jacka Kaczmarskiego 27, 02-679 Warsaw, Poland; Zbigniew.Bochenek@igik.edu.pl (Z.B.); Dariusz.Ziolkowski@igik.edu.pl (D.Z.)
4 Independent Department of Biotechnology and Molecular Biology (IDBMB), Opole University, ul. Kard. B. Kominka 6, 45-032 Opole, Poland; aklos@uni.opole.pl
5 Pixalytics Ltd., 1 Davy Road, Plymouth Science Park, Derriford, Plymouth, Devon PL6 8BX, UK; slavender@pixalytics.com
* Correspondence: bogdan@uw.edu.pl; Tel.: +48-225-520-654

Received: 15 October 2017; Accepted: 8 December 2017; Published: 11 December 2017

Abstract: Remote sensing is a suitable candidate for monitoring rapid changes in Polar regions, offering high-resolution spectral, spatial and radiometric data. This paper focuses on the spectral properties of dominant plant species acquired during the first week of August 2015. Twenty-eight plots were selected, which could easily be identified in the field as well as on RapidEye satellite imagery. Spectral measurements of individual species were acquired, and heavy metal contamination stress factors were measured contemporaneously. As a result, a unique spectral library of dominant plant species, heavy metal concentrations and damage ratios were achieved with an indication that species-specific changes due to environmental conditions can best be differentiated in the 1401–2400 nm spectral region. Two key arctic tundra species, *Cassiope tetragona* and *Dryas octopetala*, exhibited significant differences in this spectral region that were linked to a changing health status. Relationships between field and satellite measurements were comparable, e.g., the Red Edge Normalized Difference Vegetation Index (RENDVI) showed a strong and significant relationship (R^2 = 0.82; p = 0.036) for the species *Dryas octopetala*. Cadmium and Lead were below detection levels while manganese, copper and zinc acquired near Longyearbyen were at concentrations comparable to other places in Svalbard. There were high levels of nickel near Longyearbyen (0.014 mg/g), while it was low (0.004 mg/g) elsewhere.

Keywords: Svalbard; Tundra; *Cassiope tetragona*; *Salix polaris*; *Bistorta vivipara*; *Dryas octopetala*; Spectrometry; Optical sampling; RapidEye; Red edge; vegetation indices

1. Introduction

Arctic temperatures have increased, stimulating plant growth; a trend widely referred to as "the greening of the Arctic" [1–3]. However, many northern latitudes have also experienced suppressed growth known as browning. In continental regions, summer droughts and wildfires are the main

drivers of this browning trend [4,5]. In maritime regions other climatic and biotic drivers stress vegetation, e.g., frost drought [6] and ice-induced anoxia (plant damage following encasement in ground-ice). Plant damage from a changing winter climate is increasing in frequency [7,8], as winters are warming more than summers [9]. In addition, environmental pollution is affecting plant vitality in northern ecosystems [10–12], which may make plants more vulnerable to climatic change.

The absorption, transmission or reflection of the electromagnetic spectrum by plants (their pigments, biochemical features or cellular structures) can play a significant role in the long-term monitoring of ecosystem changes. Variations in plant canopy and leaf structure as well as pigment and water content can result in changing reflectance properties, even between closely related species. Thus, species identification is possible from these unique spectral properties [13]. It is known that the spectral properties of plant species depend on plant physiology, morphology or anatomy [14,15]. Only a few studies in the Arctic and boreal regions have focused on the spectral properties of single species using hyperspectral sensors [16,17]; most studies focus primarily on vegetation communities [18,19]. From the vegetation point of view, the most important role is played by pigments and nutrients (plant vitality), but survival strategies related to phenology and morphology may differ between plant species [20]. Such adaptations have a direct impact on plant properties, which can be used for remote sensing monitoring [21]. These methods are based on comparisons of absorption/reflectance features at different wavelengths [22]. Through an integration of field-based (near-ground) spectroscopy and remotely sensed data, plant vitality at different scales can be monitored. Field spectrometers, which use fiber optics and in some cases, artificial light, make it possible to obtain high-quality data which are repeatable during the day and growing seasons [23,24]. The sheer quantity of registered data from the spectrometer eliminates randomly selected signals. Application of such data is in differentiating between vegetation types and species for the production of vegetation and biomass maps [25–28]. In particular, the use of remotely sensed data in sensitive and remote Arctic areas is efficient and minimizes the environmental footprint [29].

Spitsbergen, the main island of the Svalbard archipelago in the European High-Arctic, has a long history of human disturbance, particularly extensive coal mining, which began in 1906, and from which 22.5 million tons of coal had been extracted by 1997 [12]. In recent years, the average annual extraction by the major coal mining company is 2.3 million tons [30]. Runoff from mine waste rock piles releases large concentrations of heavy metals into the surrounding areas, including aluminum (Al), zinc (Zn), manganese (Mn), cooper (Cu), nickel (Ni), iron (Fe) and arsenic (As) at phytotoxic concentrations that can have a significant negative impact on vegetation [12]. High concentrations of nickel (Ni), found in soils and plant samples at a distance from mining sites, indicate possible wind dispersal of coal dust [31].

As part of the High Arctic, Svalbard is undergoing rapid climate change [9], with warmer summer climate leading to extreme plant growth [32]. However, the winter climate is changing more than the summer climate that has led to extreme wintertime events for both animals and society [33]. The impacts of such climate events on plant cover has not yet been studied in detail, but the observed browning of some dwarf shrub species [29,34] may relate to extreme winter conditions, similar to the damage that has been documented in sub-Arctic Scandinavia [7,8].

We studied a vegetation transect in western Spitsbergen with the objectives: (1) to assess differences in spectral reflectance curves of common High-Arctic plant species from contrasting functional groups (dwarf shrubs with perennial leaves, with and without leaf yellowing in autumn; deciduous dwarf shrubs; and herbaceous plants); (2) to elucidate intraspecific variation in spectral reflectance curves and vegetation indices; (3) to evaluate whether intraspecific variation reflects plant vitality; (4) to assess whether any changes in reflectance curves may be related to pollution or climate stress; and (5) to assess how well satellite data can detect vegetation stress on the ground.

2. Study Area

The study area is located at 78.2°N and 15.6°E in proximity of Longyearbyen, the major settlement in Svalbard (Figure 1). The area is characterized by a mild and wet maritime-buffered (one of the wettest) High-Arctic climate with mean temperatures for the warmest and coldest months of 6.5 °C (July) and −15.2 °C (February) respectively, and nutrient-rich soils [27,29]. The Longyearbyen area has a long history of coal mining, which has led to contamination of soil and vegetation [9]. The vegetation is dominated by bryophyte-rich fens and marshes in the lower flat areas along the river valleys (e.g., Adventdalen), and polar willow (*Salix polaris*), white Arctic bell-heather (*Cassiope tetragona*), alpine bistort (*Bistorta vivipara*) and mountain avens (*Dryas octopetala*) on elevated, exposed and drier sites [27,35].

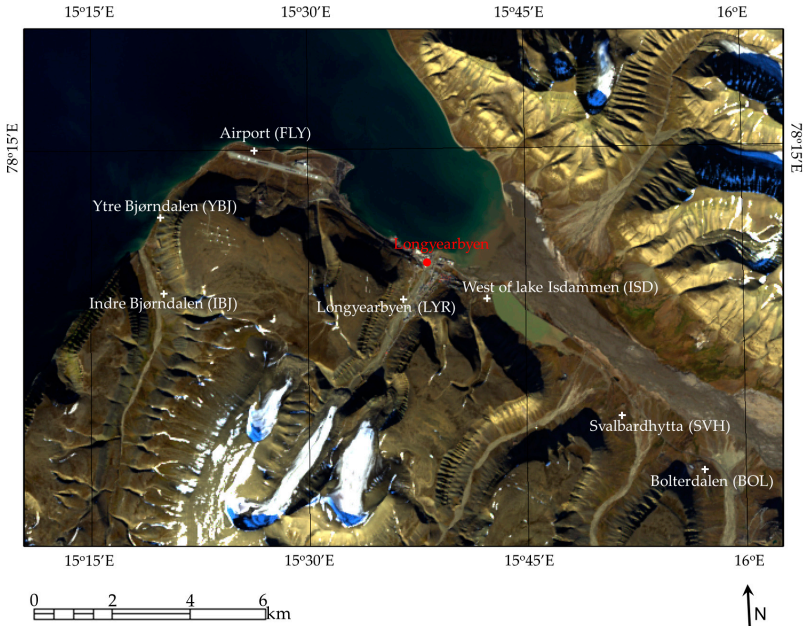

Figure 1. Sampling sites near Longyearbyen on the main island in Svalbard. YBJ, FLY and ISD sites are exposed for a direct ocean influence, and SVH and BOL are curtained areas in the Advent valley.

Data were acquired from seven sites on dry to moist tundra communities dominated by the vascular species mentioned above (Figure 1). The sites are named Bolterdalen (BOL, site1), Svalbardhytta (SVH, 2), Isdammen (ISD, 3), Longyearbyen (LYR, 4), Airport (FLY, 5), Ytre Bjørndalen (YBJ, 6), and Indre Bjørndalen (IBJ, 7). The sites BOL, IBJ, ISD, LYR and SVH and YBJ are situated in open-to-dense Dryas-dominated tundra/Moss tundra, while the FLY site is situated in an exposed area of Dryas tundra/Moist Moss tundra [27]. Four plots of 1 × 1 m were selected randomly on previous monitoring areas at each site using stratified random selection procedures. These plots are located within large patches of homogenous tundra vegetation (approximately three times larger than a RapidEye pixel, which covers 5 × 5 m), with each positioned using GPS measurements and identified by small wooden stakes.

3. Materials and Methods

3.1. In-Situ Data Collection and Processing

The field data were acquired during an in situ measurement campaign between 4 and 7 August 2015 using an ASD FieldSpec 3 spectroradiometer (ASD Inc., Longmont, CO, USA, Table 1) fit with an ASD PlantProbe [36]. The contact probe, which uses an artificial light and closed chamber for data acquisition at the leaf-level, offered comparable light conditions for all measurements. The spectrometer

measures the electromagnetic spectrum in the range of 350 to 2500 nm with the ASD white reference panel in the cap as the calibration target. Due to the ASD FieldSpec 3 acquisition method, the spectrometer was configured to average 25 measurements for each acquisition and 10 acquisitions were completed for each spectral record resulting in 250 measurements per record, affording a higher objectivity of data.

Table 1. Technical specification of an ASD FieldSpec 3 spectrometer (www.asdi.com, Boulder, CO, USA).

Spectral Range:	**350–2500 nm**
Sampling interval:	1.4 nm for 350–1000 nm 2 nm for 1000–2500 nm
Spectral resolution (Full Width Half Maximum):	3 nm at 700 nm 10 nm at 1400 nm and 2100 nm
Data collection speed:	0.1 s single spectrum acquisition 1.5 s for 10 spectra averaging
Noise equivalent delta radiance (NeDL):	1.4×10^{-9} W/cm^2/nm/sr @ 700 nm 2.4×10^{-9} W/cm^2/nm/sr @ 1400 nm 8.8×10^{-9} W/cm^2/nm/sr @ 2100 nm

The data were acquired for four species: alpine bistort (*Bistorta vivipara*), white Arctic bell-heather (*Cassiope tetragona*), mountain avens (*Dryas octopetala*) and polar willow (*Salix polaris*) in every site. These species are abundant in the High-Arctic tundra in Svalbard, and are also common in the sub-Arctic and alpine environments [35]. The measurements were carried out on green and healthy looking leaves [10,37], resulting in 24, 31, 29 and 28 distinct spectral signatures for *Bistorta vivipara*, *Cassiope tetragona*, *Dryas octopetala* and *Salix polaris* respectively.

The acquired data were exported to an ASCII file using the ASD ViewPro software for statistical analysis (Figure 2), with vegetation spectral reflectance properties checked visually using spectral reflectance curves. Two analytical approaches were applied. First, a statistical analysis was conducted to select the spectral bands that best differentiate between analyzed species. This step was achieved using stepwise linear discriminant analysis (LDA) for band selection [38] and nonparametric multivariate analysis of variance technique (NPMANOVA) to validate the ability of selected bands to successfully separate all species (measured group differences are statistically significant) [39]. Secondly, plant vitality by means of optical vegetation indices was assessed [6]. On each plot for the dwarf shrub species (*Cassiope tetragona* and *Dryas octopetala*) we measured the cover of each species following a percent scale, the health status using the color of the apex leaves of each species and finally the damage ratio of each species following the methods in Bjerke et al. [6]. The ratio of dead plants was confirmed by ecophysiological measurements such as chlorophyll fluorescence [6].

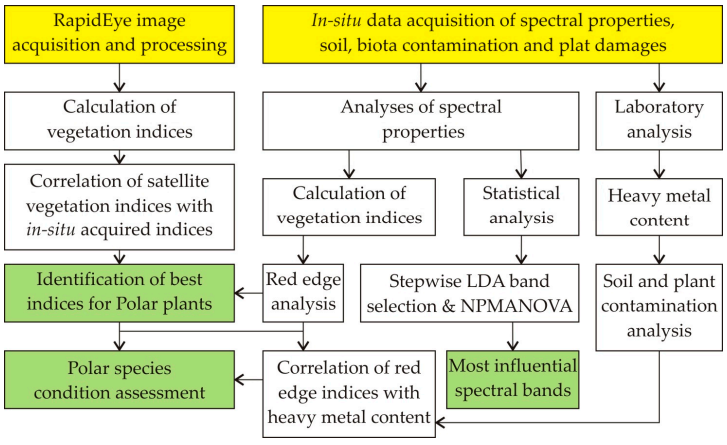

Figure 2. An overview of the pre-processing steps for statistical analysis.

Heavy metal concentrations were used as an indicator of vegetation condition. Following the methods in Klos et al. [31], leaf samples from test plots and soil samples from the upper five-centimeter top layer were taken for analysis parallel to spectrometric measurements. Collected material was dried at 323 K and stored in closed polyethylene containers. During the laboratory analysis, a 0.4 g subsample was taken from the homogenized material and mineralized in a mixture of nitric acid and hydrogen dioxide in a Speedwave Four microwave oven (Berghof, DE). Concentrations of Mn, Ni, Cu, Zn, Cd and Pb were determined via the Flame Atomic Absorption Spectroscopy (FAAS) method using an ICE 3000 (Thermo Electron Corporation, Waltham, MA, USA). To determine mercury concentrations, an AMA 254 analyzer was utilized. Detailed results are presented in an open-access paper [40].

3.2. Calculation of Vegetation Indices

Even small changes in reflectance can be measured, recorded and assigned to a specific species, allowing for species identification based solely on spectral properties. Thereby, contrasting spectral reflectance curves were used to identify species-specific spectral properties [41–43].

We used a series of vegetation indices derived from spectrometric analysis to assess the vitality of the plants (Table 2). The indices for canopy water content, red edge, broadband greenness, dry or senescent carbon and leaf pigments use wide spectral wavelength bands to assess the general vegetation condition or preciously selected pigments or building substances by narrow-band feature absorption [3,22,44], as well as to correlate field-based index values with airborne or satellite data [45,46]. All vegetation indices had a nonparametric distribution, and therefore, in order to find statistically significant ($p < 0.05$ level) indicators Kruskal-Wallis one-way analysis of variance was used to analyze relationships between visually assessed percentage of dry plants on plots (damage ratios) and heavy metal concentrations (mg/g) based on Spearman tests.

The Moisture Stress Index (MSI) is a water content vegetation index that provides a measure of the amount of water contained in the canopy foliage i.e., leaf water content [47].

Narrowband greenness indices are applicable for assessing vegetation vigor and quality of biomass. Such indices are useful when the focus is on specific aspects of plant vitality or vigor e.g., change in pigment content during the growing season. The broadband indices allow comparison of ground-based measurements with spaceborne imagery concerning condition and vitality of the vegetation, while the narrowband indices were used as indicators of plant physiology with an emphasis on how the vitality of the different species changed with heavy metal concentrations. The broadband indices chosen were the Simple Ratio [48], NDVI [3,44] and EVI [49], chosen according to the available RapidEye bands. Red edge indices are based on the steepness and location of the red edge slope, a transition from the visible red region of the electromagnetic spectrum to the near infrared (NIR) [50] that is also an area of transition from chlorophyll absorption to scattering from canopy structure. The slope and position of the red edge is sensitive to chlorophyll concentration and can shift with changes in its content, revealing information about plant stress or injury [10,50,51].

The next step was to analyze the influence of heavy metals on the red edge response, with a focus on any spectral shift of the red edge curves to the visible or near infrared. Red edge vegetation indices (REPI, MRENDVI, MRESR, and RENDVI) were calculated and the relationship between changes in red edge and heavy metal concentrations were investigated using the Spearman correlation. The most used red edge vegetation index is the Red Edge Normalized Difference Vegetation Index—RENDVI (Table 2). The relative cover of healthy vs. damaged vegetation was estimated on an area basis, viz. plants with green shoots were considered healthy, whereas shoots with brown or grey leaves were considered damaged [6]. This damage was shown to be caused by stressful conditions during winter [6]. Usually, lower NDVI values (<0.6) are measured for species and sites operating within more adverse environmental conditions, while species and sites in good health had a NDVI of 0.6–0.7 with species and sites in very good condition having NDVI values > 0.7 [6,52].

Table 2. Vegetation indices calculated from the sampled reflectance curves.

Name	Equation	Explanation	Comments	Source
Canopy water content				
Moisture Stress Index	$MSI = \frac{R_{1599}}{R_{819}}$	Water content	High values indicate water stress	[47]
Red edge vegetation indices				
Red Edge Normalized Difference Vegetation Index	$\mathrm{RENDVI} = \frac{R_{750}-R_{705}}{R_{750}+R_{705}}$	NDVI based on red edge spectral range	Good condition 0.2–0.9	[50,51]
Modified Red Edge Normalized Difference Vegetation Index	$MRENDVI = \frac{R_{750}-R_{705}}{R_{750}+R_{705}-2*R_{445}}$	Modification of RENDVI taking into account leaf specular reflection	Good condition 0.2–0.7	[51,53]
Modified Red Edge Simple Ratio (mSR_{705})	$\mathrm{MRESR} = \frac{R_{750}-R_{445}}{R_{705}-R_{445}}$	Red edge modification of SR.	Good condition 2–8	[46,51]
Red Edge Position Index	$\mathrm{REPI} = (R_{670} + R_{780})/2$ $\mathrm{REPI} = 700 + 40((R_{670} - R_{700})/(R_{740} - R_{700}))$	Chlorophyll shifts of red edge	Good condition 700–730 nm	[54,55]
Broadband greenness				
Simple Ratio	$\mathrm{SR} = \frac{R_{800}}{R_{680}}$	General plant condition	Increase with better condition	[56]
Normalized Difference Vegetation Index	$\mathrm{NDVI} = \frac{R_{800}-R_{680}}{R_{800}+R_{680}}$	Biomass content	Increase with better condition	[3,44]
Enhanced Vegetation Index	$EVI = 2.5 * \left[\frac{R_{800}-R_{680}}{1+R_{800}+6 * R_{680}-7.5 * R_{450}}\right]$	NDVI with a correction of soil reflectance	Increase with better condition	[57]
Dry or senescent carbon				
Plant Senescence Reflectance Index	$PSRI = \frac{R_{680}-R_{500}}{R_{750}}$	Chlorophyll/ carotenoids ratio	Good condition −0.1–0.2	[58]
Leaf pigments				
Carotenoid Reflectance Index	$CRI1 = \frac{1}{R_{510}} - \frac{1}{R_{550}}$	Carotenoids/ chlorophyll ratio	Good condition 1–12	[59]
Carotenoid Reflectance Index	$CRI2 = \frac{1}{R_{510}} - \frac{1}{R_{700}}$		Good condition 1–11	[59]
Anthocyanin Reflectance Index	$\mathrm{ARI1} = \frac{1}{R_{550}} - \frac{1}{R_{700}}$	Anthocyanin amount	Increase in pigment means	[60]
Anthocyanin Reflectance Index	$ARI2 = R_{800} * (\frac{1}{R_{550}} - \frac{1}{R_{700}})$	Anthocyanin amount	New growth of leaves or senescence	[60]

3.3. Remotely Sensed Data from RapidEye

The RapidEye sensor acquired data in the same week (5 August 2014) as the leaf-level-based ASD FieldSpec measurements, whose narrow bands were averaged to the spectral resolution of the RapidEye spectral band widths i.e., a red band from 635 to 680 nm, red edge band from 690 to 730 nm and NIR band from 760 to 850 nm (www.planet.com, Table 3.) that differs somewhat from the original formula by Gitelson and Merzlyak [50].

Atmospheric correction was carried out using the "Dark object subtraction" routine in ENVI 5.4. This routine searches each band for the pixel with the darkest value. Further, assuming that dark objects reflect no light, any value greater than zero is assumed to be contaminated by atmospheric scattering. Therefore, the scattering is removed by subtracting this dark value from every pixel in each of the 6 RapidEye bands (www.harrisgeospatial.com).

The RapidEye data was used to assess how well satellite-based sensors can detect possible stress in the different plots and vegetation communities, in comparison to the leaf-level ASD field measurements.

Table 3. RapidEye System technical data (www.planet.com).

Mission Characteristic	Information
Number of Satellites	5
Spacecraft Lifetime	Over 7 years
Orbit Altitude	630 km in Sun-synchronous orbit
Equator Crossing Time	11:00 a.m. local time (approximately)
Sensor Type	Multi-spectral push broom imager
Spectral Bands	Blue (440–510 nm), Green (520–590 nm), Red (630–685 nm), Red Edge (690–730 nm), NIR (760–850 nm)
Ground Sampling Distance (nadir)	6.5 m
Pixel size (orthorectified)	5 m
Swath Width	77 km
On board data storage	Up to 1500 km of image data per orbit
Revisit time	Daily (off-nadir)/5.5 days (at nadir)
Image capture capacity	5 million km^2/day
Camera Dynamic Range	12 bit

3.4. Statistical Analysis

The statistical analyses were conducted using the R software [61]. Before employing stepwise band selection using LDA, all spectral measurements went through an analysis aimed at removing spectral bands that are highly correlated; performed by calculating the Spearman correlation coefficient between each band and its direct neighboring bands. Bands with correlation coefficients higher that 0.98 were removed from the dataset. This step is crucial to any analysis using LDA, because redundancy introduced by highly correlated bands can significantly deteriorate the ability to correctly choose variables.

After correlated bands were removed, the remaining data were used as an input to stepwise LDA analysis, using the using *klaR* [62] and *MASS* [63] packages, aimed at finding bands that best differentiate between species (based on the ability to correctly match species in feature space, and measuring it using correctness statistics) [38]. To validate the ability of selected bands to separate classes, the bands selected during stepwise LDA were also subject to NPMANOVA. The NPMANOVA test was developed to tackle some of the limitations of the multivariate analysis of variance (MANOVA) tests, such as the requirement for datasets to follow a normal distribution. It is a non-parametric test that works well for non-normally distributed datasets (providing both datasets are similarly distributed) and allows for the use of any dissimilarity measure between groups. Moreover, NPMANOVA is tolerant towards non-independent variables, which is useful when considering analyses conducted on spectra where neighboring bands are usually highly correlated with each other. Besides a *p*-value, this test also delivers a F-ratio that is a measure of group separation. The F-ratio is used to assess group separation with a high F-ratio indicating pronounced group separation, while a low F-ratios indicates weak group separation (providing differences are significant) [39]. The NPMANOVA statistical significance is computed by permutation of the group memberships. NPMANAOVA was conducted using the function "adonis" from the package *vegan* [64]. Based on a methodology presented in Jones et al. [65], the analysis was conducted on all collected spectral bands (from 400 to 2500 nm) and also for specific spectral ranges to further identify the most influential spectral regions. The spectral ranges characterized the following vegetation parameters: 400–500 nm (pigment absorption), 501–550 nm (chlorophyll reflection), 551–680 nm (pigment absorption), 681–740 nm (red edge transition), 741–1100 nm (biogeochemical), 1101–1400 nm (transitional) and 1401–2400 nm (biogeochemical).

4. Results

4.1. Differences between Species'

The spectral reflectance curves of *Bistorta vivipara*, *Salix polaris*, *Cassiope tetragona* and *Dryas octopetala* using data from all sites are presented in Figure 3. The curves of *Cassiope tetragona* and *Dryas octopetala* differed in shape from the two other species in the 700 to 1000 nm range (Figure 3), while in the 850 to 1000 nm range all species differed from each other.

Analysis performed across the whole spectral range (400–2500 nm) resulted in the selection of 17 spectral bands (Table 4). The LDA correctness rate was 0.99, confirming their importance in differentiating between species, while the NPMANOWA F-ratio was 101 at a significance level of 0.05 implying a good separation of classes in the feature space.

The analysis was repeated for specific spectral ranges (Table 5). For all analyzed ranges, the results of the NPMANOVA test were significant ($p < 0.05$). The 400 to 500 nm spectral region allows for an assessment of pigment interaction with light [37,51]. In this region, 12 bands were found to best characterize species that resulted in a 0.90 correctness rate during the LDA stepwise selection of bands. In addition, the NPMANOVA F-ratio was 18.8 that indicated a modest separation of species. Moving onto the second investigated spectral region (501–550 nm), 6 bands were selected with an F-ratio of 29.77 and correctness rate of 0.68. In the third spectral region (551–680 nm) 9 spectral bands had an F-ratio of 40.6 and correctness rate of 0.86. Similarly, 9 bands were found to be important in the spectral region located across the red edge (681–740 nm). Selected bands here have an F-ratio of 24.4 and a correctness rate of 0.90. Bands in the VIS-NIR region gave varying correctness rates (depending on spectral region), and produced a high number of important bands that were evenly distributed throughout the regions. The fifth (741–1100 nm) and the sixth (1101–1400 nm) spectral regions provided only 3 and 4 important bands, respectively.

Table 4. Spectral bands providing best separation of species (analysis conducted on whole spectrum; NPMANOVA F-ratio 101 at significance level $p < 0.05$).

Spectral range (nm)	400–2500
Selected bands (nm)	400, 403, 405, 407, 408, 409, 411, 413, 414, 415, 427, 435, 501, 1457, 1499, 2135, 2296

Analysis performed on all spectral bands, and specific spectral ranges, showed that the 1401–2400 nm region is slightly better at differentiating between species than a data set composed of all spectral bands; achieving a higher F-ratio and similar correctness statistic.

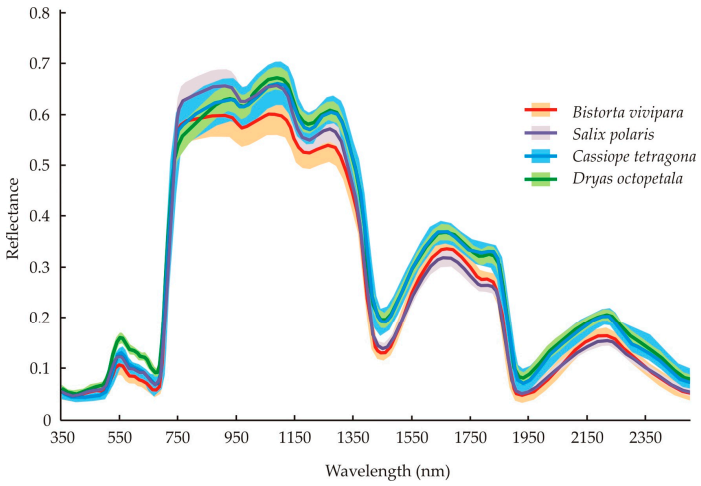

Figure 3. Average and standard deviation (strip) of spectral reflectance curves of analyzed species.

Analysis conducted on the VIS and NIR region provided high numbers of important bands, but they were characterized by significantly lower F-ratios and correctness rates. The worst performing results were found for the 501–500 nm region, with the lowest correctness rate, and 741–1100 nm region, with the lowest F-ratio. After the 1401–2400 nm region, the best regions were 400–500 nm, 681–740 nm, 1101–1400 nm and 551–680 nm. Comparing the band selection results for the whole spectrum and predetermined spectral regions it was noticeable that the bands selected using all the available data were almost exclusively in 2 regions: 400–500 nm and 1401–2400 nm.

Table 5. Best bands found within selected spectral regions.

Spectral Range	400–500	501–550	551–680	681–740	741–1100	1101–1400	1401–2400
Selected bands (nm)	405	501	584	682	745	1101	1401
	412	507	587	686	753	1200	1499
	430	509	601	693	999	1386	1801
	448	510	615	695		1398	1931
	451	520	618	697			2135
	458	523	630	699			2297
	461		657	726			2359
	467		666	736			2399
	473		677	740			
	477						
	498						
	499						
F-ratio	18.80 *	29.77 *	40.60 *	24.40 *	12.21 *	35.05 *	105.78 *
Correctness	0.928	0.6894	0.8659	0.90	0.75	0.89	0.98

* Differences are statistically significant ($p < 0.05$).

4.2. Plant Species Condition Assessment

The broadband vegetation indices indicate the overall health, e.g., the leaf-level spectrometer measured NDVI values a very good vegetation condition (NDVI > 0.7) for *Salix polaris* and *Bistorta vivipara*, and good for *Dryas octopetala* (NDVI > 0.6; Table 6). For *Cassiope tetragona*, lower NDVI values (<0.6) indicate a reduced vegetation health. Similarly, the EVI index values showed good condition for *Salix polaris*, *Dryas octopetala* and *Bistorta vivipara*, and quite good for *Cassiope tetragona*. NDVI values from RapidEye show comparable results to ground-based NDVI values (Table 6). However, some of the sites (ISD) showed lower NDVI and red edge indices compared to the ASD FieldSpec.

Table 6. Values of vegetation indices: Normalized Difference Vegetation Index (NDVI), Enhanced Vegetation Index (EVI), Plant Senescence Reflectance Index (PSRI), and Moisture Stress Index (MSI).

Species	Research Site	ASD Vegetation Index				NDVI
		NDVI	EVI	PSRI	MSI	RapidEye
Bistorta vivipara	BOL	0.73	0.73	0.05	0.49	0.213
	FLY	-	-	-	-	-
	IBJ	0.81	0.84	0.01	0.49	0.135
	ISD	0.80	0.85	0.00	0.51	0.097
	LYR	0.80	0.79	0.00	0.51	0.160
	SVH	0.77	0.79	0.03	0.48	0.096
	YBJ	0.79	0.81	0.00	0.49	-

Table 6. *Cont.*

Species	Research Site	ASD Vegetation Index				NDVI
		NDVI	EVI	PSRI	MSI	RapidEye
Cassiope tetragona	BOL	0.74	0.72	0.05	0.58	0.213
	FLY	0.58	0.49	0.16	0.74	-
	IBJ	0.76	0.71	0.03	0.64	0.135
	ISD	0.72	0.69	0.05	0.67	0.097
	LYR	0.47	0.34	0.26	0.77	0.160
	SVH	0.55	0.38	0.17	0.97	0.096
	YBJ	0.62	0.52	0.14	0.73	-
Dryas octopetala	BOL	0.75	0.86	0.03	0.54	0.213
	FLY	0.57	0.53	0.10	0.59	-
	IBJ	0.68	0.78	0.04	0.62	0.135
	ISD	0.71	0.68	0.03	0.53	0.097
	LYR	0.72	0.69	0.02	0.66	0.160
	SVH	0.71	0.69	0.03	0.51	0.096
	YBJ	0.72	0.73	0.03	0.51	-
Salix polaris	BOL	0.74	0.74	0.01	0.54	0.213
	FLY	0.50	0.40	0.08	0.53	-
	IBJ	0.83	0.86	0.00	0.43	0.135
	ISD	0.77	0.69	0.01	0.48	0.097
	LYR	0.75	0.72	0.02	0.58	0.160
	SVH	0.72	0.74	0.01	0.47	0.096
	YBJ	0.74	0.75	0.02	0.53	-

The Plant Senescence Reflectance Index (PSRI) values showed that all species were in good condition; however, for *Cassiope tetragona* the PSRI showed an increased value, indicating that this species was not in senescence stage and so time lagged compared to the other species. MSI indicated that water stress was not present. Calculating vegetation indices for each test site separately provided information on spatial variation in index values (Table 7), indicating local differences in health status of the tested plant species. The vegetation indices (Tables 7 and 8) suggest that B*istorta vivipara* had the best health condition at the ISD site and lowest at BOL and SVH. *Cassiope tetragona* showed good health at three sites (BOL, IBJ and ISD), and severely reduced health at three other sites (FLY, LYR and SVH). *Dryas octopetala* show largely the same trend, with the highest values at BOL and the lowest were at FLY and SVH. For *Salix polaris*, the highest index values were measured at the IBJ and BOL sites, while the lowest were at FLY and LYR. Thus, all species show moderate to large variation in health within short distances (Table 7).

Based on these indices (Table 8), as well as heavy metal concentrations in the soil, the best conditions for *Bistorta vivipara* was observed at the ISD and LYR plots while the worst at the BOL and SVH sites.

On large homogenous plots of BOL, FLY, IBJ, ISD, LYR, SVH, which are covered by the species *D. octopetala*, *a* strong relationship (R^2 = 0.82 p = 0.036) was found between the in situ measured RENDVI and the RapidEye extracted RENDVI (Figure 4, Table 9).

Table 7. Variability of vegetation indices (highest standard deviations between measurement sites); Simple Ratio (SR), Modified Red Edge Simple Ratio (mSR_{705}), Carotenoid Reflectance Indices 1, 2 (CRI 1 and 2), and the Anthocyanin Reflectance Indices 1, 2 (ARI 1 and 2).

Species	Research Site	Vegetation Index					
		SR	**mSR 705**	**CRI 1**	**CRI 2**	**ARI 1**	**ARI 2**
Bistorta vivipara	BOL	6.50	3.51	5.66	10.23	4.57	2.72
	IBJ	9.36	3.43	7.27	11.95	4.68	2.96
	ISD	9.01	4.26	6.08	8.03	1.95	1.16
	LYR	8.80	3.46	8.51	9.66	1.15	0.65
	SVH	7.66	3.15	7.96	10.11	2.15	1.34
	YBJ	8.32	3.72	6.02	8.11	2.09	1.20
Cassiope tetragona	BOL	5.61	2.35	7.40	10.16	2.76	1.46
	FLY	4.90	2.37	6.43	9.00	2.57	1.27
	IBJ	5.76	2.41	7.81	9.98	2.17	1.14
	ISD	6.48	2.75	7.67	9.56	1.89	1.01
	LYR	4.20	2.13	6.54	10.04	3.50	1.66
	SVH	4.57	2.19	7.01	10.54	3.52	1.54
	YBJ	6.03	2.31	7.63	10.43	2.80	1.61
Dryas octopetala	BOL	6.95	3.37	5.70	6.86	1.17	0.74
	FLY	4.42	2.05	5.72	8.54	2.82	1.49
	IBJ	5.58	2.81	4.66	5.61	0.96	0.60
	ISD	5.48	2.63	5.84	6.96	1.12	0.64
	LYR	4.88	2.44	4.87	6.02	1.15	0.63
	SVH	6.01	2.65	6.40	7.84	1.44	0.92
	YBJ	5.17	2.52	4.96	6.50	1.54	0.93
Salix polaris	BOL	8.46	3.71	7.97	9.76	1.80	1.04
	FLY	5.81	2.50	8.41	9.86	1.44	0.77
	IBJ	8.42	4.13	7.34	8.14	0.80	0.45
	ISD	7.55	3.80	6.24	7.36	1.12	0.69
	LYR	7.21	3.74	6.53	8.70	2.16	1.10
	SVH	6.43	3.13	6.36	8.07	1.71	0.90
	YBJ	9.17	4.39	7.51	8.01	0.51	0.30

Table 8. Calculated red edge vegetation indices from ASD FieldSpec and the RapidEye image (REi) as well as the heavy metals concentrations (mg/g) in plants and soil. Column headings: (1)—REPI (nm), (2)—RENDVI, (3)—MRENDVI, (4)—MRESR. Damage ratio – percent of damaged plants. n.a. = not applicable, n.m. = not measured.

	Sites	Red Edge Vegetation Index				REi	Heavy Metal Concentrations (mg/g)							Damage
		(1)	(2)	(3)	(4)	(2)	Cu	Mn	Ni	Pb	Zn	Cd	Soil	Ratio (%)
Soil	BOL	n.a.	n.a.	n.a.	n.a.	0.12	0.035	0.80	0.025	0.035	0.230	0.005	1.129	n.a.
	FLY	n.a.	n.a.	n.a.	n.a.	-	0.031	0.84	0.021	0.046	0.152	0.004	1.094	n.a.
	IBJ	n.a.	n.a.	n.a.	n.a.	0.07	0.033	0.69	0.017	0.042	0.169	0.004	0.955	n.a.
	ISD	n.a.	n.a.	n.a.	n.a.	0.03	0.036	0.68	0.014	0.038	0.207	0.004	0.979	n.a.
	LYR	n.a.	n.a.	n.a.	n.a.	0.03	0.055	0.32	0.003	0.042	0.148	0.001	0.569	n.a.
	SVH	n.a.	n.a.	n.a.	n.a.	0.04	0.038	0.85	0.007	0.040	0.229	0.001	1.165	n.a.
	YBJ	n.a.	n.a.	n.a.	n.a.	-	0.029	0.580	0.010	0.049	0.183	0.001	0.852	n.a.
Bistorta vivipara	BOL	719	0.46	0.54	3.31	0.12	n.m.	n.m.	n.m.	n.m.	n.m.	n.m.	1.129	0.00
	FLY	-	-	-	-	-	n.m.	n.m.	n.m.	n.m.	n.m.	n.m.	1.094	0.00
	IBJ	718	0.46	0.52	3.20	0.07	n.m.	n.m.	n.m.	n.m.	n.m.	n.m.	0.955	0.00
	ISD	719	0.51	0.59	3.94	0.03	n.m.	n.m.	n.m.	n.m.	n.m.	n.m.	0.979	0.00
	LYR	717	0.46	0.53	3.22	0.03	n.m.	n.m.	n.m.	n.m.	n.m.	n.m.	0.569	0.00
	SVH	717	0.43	0.49	2.96	0.04	n.m.	n.m.	n.m.	n.m.	n.m.	n.m.	1.165	0.00
	YBJ	718	0.47	0.55	3.47	-	n.m.	n.m.	n.m.	n.m.	n.m.	n.m.	0.852	0.00
Cassiope tetragona	BOL	715	0.33	0.38	2.24	0.12	0.006	0.29	0.010	0.004	0.028	0.001	1.129	22.43
	FLY	715	0.33	0.39	2.26	-	0.007	0.12	0.011	0.004	0.039	0.001	1.094	14.82
	IBJ	715	0.35	0.39	2.30	0.07	0.006	0.20	0.012	0.004	0.023	0.001	0.955	14.68
	ISD	716	0.38	0.44	2.60	0.03	0.006	0.39	0.013	0.004	0.026	0.001	0.979	29.26
	LYR	715	0.29	0.34	2.05	0.03	0.006	0.26	0.012	0.004	0.030	0.001	0.569	18.24
	SVH	715	0.30	0.36	2.10	0.04	0.005	0.45	0.013	0.004	0.030	0.001	1.165	10.96
	YBJ	714	0.33	0.38	2.21	-	0.004	0.20	0.011	0.004	0.017	0.001	0.852	18.24
Dryas octopetala	BOL	719	0.44	0.52	3.18	0.12	n.m.	n.m.	n.m.	n.m.	n.m.	n.m.	1.129	9.55
	FLY	713	0.28	0.33	1.97	-	n.m.	n.m.	n.m.	n.m.	n.m.	n.m.	1.094	10.79
	IBJ	717	0.38	0.45	2.67	0.07	n.m.	n.m.	n.m.	n.m.	n.m.	n.m.	0.955	0.00
	ISD	716	0.36	0.43	2.50	0.03	n.m.	n.m.	n.m.	n.m.	n.m.	n.m.	0.979	14.37
	LYR	715	0.33	0.40	2.33	0.03	n.m.	n.m.	n.m.	n.m.	n.m.	n.m.	0.569	15.82
	SVH	716	0.38	0.43	2.52	0.04	n.m.	n.m.	n.m.	n.m.	n.m.	n.m.	1.165	0.00
	YBJ	716	0.35	0.41	2.41	-	n.m.	n.m.	n.m.	n.m.	n.m.	n.m.	0.852	4.27
Salix polaris	BOL	719	0.49	0.55	3.49	0.12	0.004	0.31	0.021	0.004	0.29	0.001	1.129	0.00
	FLY	714	0.35	0.41	2.37	-	0.0032	0.14	0.014	0.004	0.05	0.001	1.094	0.00
	IBJ	719	0.50	0.59	3.84	0.07	0.0044	0.43	0.015	0.004	0.35	0.001	0.955	0.00
	ISD	719	0.48	0.56	3.59	0.03	0.0049	0.37	0.019	0.004	0.32	0.001	0.979	0.00
	LYR	719	0.48	0.56	3.52	0.03	0.0045	0.63	0.016	0.004	0.45	0.001	0.569	0.00
	SVH	717	0.42	0.50	2.97	0.04	0.0039	0.32	0.016	0.004	0.26	0.001	1.165	0.00
	YBJ	720	0.53	0.61	4.09	-	0.0038	0.19	0.015	0.004	0.20	0.001	0.852	0.00

Table 9. Calculated Spearman correlation of Vegetation Indices with damage ratios and heavy metal concentrations (mg/g) in plants and soil. Test conducted at significance level <0.05.

Species	Vegetation Index	RENDVI_REi	Damage Ratio	Heavy Metal Concentrations						
				Cu	Mn	Ni	Pb	Zn	Cd	Soil
Cassiope tetragona	RENDVI_REi	-	−0.30	−0.05	−0.30	−0.70	0.00	−0.15	0.00	0.30
	REPI (nm)	−0.71	0.34	0.54	0.47	0.47	0.00	0.27	0.00	0.27
	RENDVI	−0.10	0.35	0.47	−0.11	−0.11	0.00	−0.54	0.00	0.04
	MRENDVI	−0.10	0.28	0.65	−0.24	−0.11	0.00	−0.28	0.00	0.11
	MRESR	−0.10	0.29	0.67	−0.16	−0.11	0.00	−0.31	0.00	0.14
	CRI2	0.50	−0.25	**−0.92** **	0.49	0.13	0.00	−0.23	0.00	0.18
Dryas Octopetala	RENDVI_REi	-	−0.56	−0.60	−0.50	0.00	0.00	0.00	0.00	0.30
	REPI (nm)	0.82	−0.52	-	-	-	-	-	-	0.26
	RENDVI	0.87	−0.56	-	-	-	-	-	-	0.51
	MRENDVI	0.82	−0.48	-	-	-	-	-	-	0.38
	MRESR	**0.90** *	−0.56	-	-	-	-	-	-	0.43
	CRI2	−0.30	0.09	-	-	-	-	-	-	0.71
Salix polaris	RENDVI_REi	-	-	−0.60	−0.50	0.00	0.00	−0.30	0.00	0.30
	REPI (nm)	0.00	-	0.32	0.22	0.22	0.00	0.32	0.00	−0.63
	RENDVI	0.56	-	0.13	0.14	0.09	0.00	0.25	0.00	−0.49
	MRENDVI	−0.15	-	0.23	0.36	−0.02	0.00	0.40	0.00	−0.74
	MRESR	−0.20	-	0.25	0.32	0.00	0.00	0.36	0.00	−0.68
	CRI2	0.70	-	−0.32	−0.25	−0.14	0.00	−0.14	0.00	0.18

* = Correlation is significant at the 0.05 (2-tailed). ** = Correlation is significant at the 0.01 (2-tailed). Accordingly, the following sites saw the best and worst condition (respectively) for the other species: *Cassiope tetragona*—IBJ/ISD and LYR/SVH; *Dryas octopetala*—BOL and FLY; *Salix Polaris*—IBJ and FLY. The highest heavy metal values in vegetation and soil were found at the SVH, FLY and BOL sites while the lowest were found at LYR and IBJ (Table 8). The heavy metal concentrations in the plants are significantly lower compared to the upper layers of the soil (Table 8).

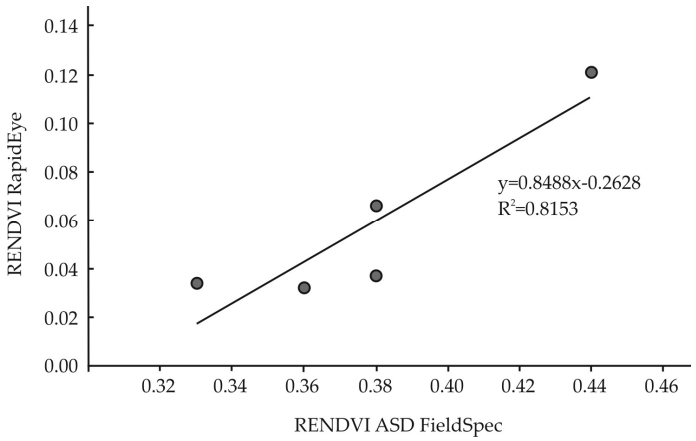

Figure 4. The relationship between the Red Edge NDVI (RENDVI) extracted from the RapidEye satellite image and the field-acquired (ASD FieldSpec) RENDVI for the species *D. octopetala* was analyzed for large homogenous plots without any other components, e.g., large stones/rocks or dry roots that could change the signal detected by the satellite sensor. Each point represents an individual measurement plot with BOL, IBJ, ISD, LYR and SVH included (Table 8).

5. Discussion

The main purpose of the study was to assess spectral reflectance curve differences for common Arctic plants from contrasting functional groups. The results indicated the electromagnetic spectrum spectral regions (Tables 4 and 5) that should be further investigated regarding their connection with plant traits linked to both the pigments within and substances covering the leaves.

NPMANOVA was used to assess a spectral regions' ability to differentiate species, and it was found that the F-ratio for the whole spectrum was smaller than that for spectral range

providing the best separation; 101 compared to 105.78 for 1401–2400 nm. Similar ranges of high correctness (above 0.90, Table 5) were achieved by Kycko [66] for dominant alpine species within the High Tatras (Poland). Some of the most significant ranges overlapped with the Kycko [66] research: 448–499 nm (Kycko [64] 446–506 nm); 682–699 nm (Kycko [66] 623–695 nm); 1801–2399 nm (Kycko [66] 1801–2500 nm). However, overall, it was concluded that the short wave infrared (SWIR, 1401–2400 nm) was most differentiating. Alternatively Clark et al. [38] found that for tropical tree species the VIS and NIR were most important with an F-ratio of 180 for the whole spectrum and 195 for the NIR. The VIS and NIR regions were also found to be most important by Jones et al. [65], whose research focused on tree species differentiation using spectroscopy. While similar research methodologies were used, it is worth noting that both Clark et al. [38] and Jones et al. [66] performed their measurements in a laboratory setting using leaf stacks while this research used a contact probe that measures the spectral signal without taking BRDF effects into account [67]. Therefore, while promising, results considering the SWIR spectral region might be misleading because of the known sensitivity of SWIR bands to BRDF related effects [67]. Moreover, analyses made on spectra collected in the SWIR region (1400–1550 nm and 1850–2000 nm) using airborne or satellite platforms are problematic due to the effects of atmospheric water vapor on measured signals.

Overall, dwarf shrubs such as the species *C. tetragona* and *D. octopetala* [6] have varying spectral shapes in the 700 nm to ~1000 nm spectral range compared with the alpine bistort *B. vivipara* and polar willow *S. polaris*. Damage ratios for *C. tetragona* and *D. octopetala* appeared not to be good indicators for vitality, but only the green leaves were measured. Therefore an approach that measures the whole plot might be a better future approach and provide improved results basing on better detectors, e.g., WorldView4. The correlation table (Table 9) indicates that the red edge indices together with CRI2 for *D. octopetala* showed higher negative correlations concerning damage ratios than *C. tetragona*. However, *C. tetragona* showed higher negative correlation for CRI2 for some of the heavy metals such as Cu.

Analysis, using existing vegetation indices, showed that *Bistorta vivipara* had minimal differences between sites, indicating that the other three species may be better environmental indicator species, i.e., show increased spectral variations linked to changes in the environment. The species *D. octopetala* and *C. tetragona* showed medium to large differences, in terms of standard deviation (Table 7), between sites indicating that these two species might be the best indicators for environmental stress in Svalbard (Figure 3); also reported by Bjerke et al. [6].

Research by Tømmervik et al. [10] at an air polluted area in the eastern part of North Norway, near the Nickel smelters in Russia, showed that the heath dominating dwarf shrub *Empetrum nigrum* had similar satellite values in the RENDVI region as *C. tetragona* in this study; curves skewed towards the blue part of the spectrum ("blue shift"). The concentrations of heavy metal were of the same magnitude (>10 μg/g) in both places [10,31,40]. Baret et al. [68] showed the existence of a strong correlation between the blue shift and the severity of damage to vascular plants, mosses and lichens. In addition, research within the northern boreal tundra of the Kola Peninsula (Russia) showed that plants exposed to the air pollution impacts of SO_2 and heavy metals such as Cu and Ni showed the same blue shift [66]. Therefore, RENDVI values may be usable an indication of stress since and *C. tetragona* may be more vulnerable than others to environmental stress [10].

Near Longyearbyen there were noticeably higher concentrations of Ni (0.014 mg/g) compared to the rest of Svalbard (0.004 mg/g) [40]. Other macro-, and microelements are at a similar level in the areas surrounding Longyearbyen and the natural areas of the Advent valley: 0.307 mg/g Mn, 0.050 mg/g Cu and 0.151 mg/g Zn. Although plant roots accumulate poisonous ions in cell walls, vacuoles and other places, this may not have a significant influence on plant physiology [31,69]. *Salix polaris* is characterized by the strong bioaccumulation of Zn, with concentrations of Cd and Pb at the detection level (0.0008 mg/g of Cd and 0.0044 mg/g Pb); as Cd and Pb are toxic heavy metals, the concentrations confirm that *S. polaris* isn't significantly affected by heavy metals in the concentration levels found here.

The increased heavy metal concentrations in *Cassiope tetragona* found at SVH might have impacted vegetation condition, highlighted by a reduced RENDVI from ASD as well as the vegetation indices extracted from RapidEye (Tables 6 and 8; Figure 4). Damage ratios for *C. tetragona* (Table 9) were highest in BOL and ISD, which correlates with the red edge indices measured in BOL but not so well in ISD. Statistical analysis of the relationships between damage ratios and the different indices (Table 9) indicated that the red edge indices, together with CRI2, for *D. octopetala* showed higher negative correlations concerning damage ratios than *C. tetragona*. However, *C. tetragona* showed higher negative correlations between CRI2 and some of the heavy metals such as Cu.

The strong relationship (R^2 = 0.82 p = 0.036) between in situ measured RENDVI and the space-borne RENVDI showed that this red edge-based vegetation index may be scaled up from the surface to space, and measurements of *D. octopetala* indicated that it could be the best species for up-scaling since many of the red edge indices (Table 9) were highly correlated with each other; albeit MESR. Also the RENDVI from RapidEye showed a relatively high-negative, but not significant, correlation with the Ni content in *C. tetragona*. However, a more rigorous procedure for up-scaling has to be undertaken in order to conclude more on this issue. Also, the RENDVI index was originally designed for hyperspectral sensors and so is sensitive to small changes in the vegetation red edge, and therefore to canopy foliage and senescence [50,51]. Since several satellite sensors are equipped with red edge bands, these narrowband indices could be used to detect subtle changes in vegetation health [10]. *Dryas octopetala* and *Cassiope tetragona* are both common and characteristic species in the prostrate dwarf shrub tundra in the Circumpolar Arctic region [25,27], and so this approach and species may be applicable to large area space-borne mapping and monitoring.

6. Conclusions

The aim of the study was to test the application of remote sensing methods to polar vegetation. Four different species were analyzed within seven measurement sites on Svalbard and the study verified that, using remote sensing methods and statistical analyses, polar plant species can be distinguished on the basis of their spectral properties.

The spectral ranges were identified through statistical analysis of species' spectral reflectance curves acquired for different measurement areas. Such information was complemented by remote sensing vegetation indices showing that all index values were in optimal ranges; according to the literature. Overall, the results suggest *Bistorta vivipara* and *Salix polaris* were in the best health, followed by *Cassiope tetragona* and *Dryas octopetala* with moderate health; likely caused by mid-winter warming events followed by extreme cold and icy conditions combined with shallow snow depths [6,10,11,33]. In addition, pollutants from the mining industry may also have contributed to reduced plant vitality that was more pronounced for *Cassiope tetragona*.

There were significant differences between measurements acquired at test sites exposed to a direct oceanic influence, and curtailed in areas such as the Advent valley, both in terms of the shape of the species' reflectance curves and calculated vegetation indices. The vegetation indices showed that *Cassiope tetragona* and *Dryas octopetala* are the best indicator species for different environmental stressors in Svalbard; these species are also found elsewhere in the Arctic. The strong relationship (R^2 = 0.82 p = 0.036) between in situ measured RENDVI and the space-borne RENVDI showed that this red edge-based vegetation index may be scaled up from surface measurements to space, and measurements of the species *D. octopetala* indicated that it is the best species for up-scaling. The issue should be developed on more accurate satellite data, e.g., WorldView4. An increased number of measurements in the field, and further analysis, has to be undertaken before more comprehensive conclusions can be made in terms of differentiating between heavy metals and climatic effects reducing plant vitality.

Acknowledgments: Research has been carried out under the Polish-Norwegian Research Programme of the Polish National Centre for Research and Development (NCBiR), project: *Ecosystem stress from the combined effects of winter climate change and air pollution—how do the impacts differ between biomes? (WICLAP)*, No. POL-NOR/198571/83/2013 and the theme No. 501-D119-64-0180200-15 were financed from grants for science awarded by the Polish Ministry of Science and Higher Education. The Svalbard environmental protection fund supported parts of the work done by the Norwegian team through the project: 17/37 Vegetation damage caused by extreme winters. The EU Cost Action Optimise (ES1309) network and the ArcticBiomass network (ArcticBiomass Grant No. RCN 227064 and SvalbardBiomass Grant No. RCN 270992) are acknowledged for assistance and help concerning knowledge and interpretation of the spectrometer data.

Author Contributions: Bogdan Zagajewski, Hans Tømmervik, Jarle W. Bjerke, Zbigniew Bochenek, Andrzej Kłos, Dariusz Ziółkowski conceived and designed the experiments and performed the field measurements; Bogdan Zagajewski (spectrometric measurements), Hans Tømmervik (plant traits, RapidEye and statistical analyses), Jarle W. Bjerke (plant traits, RapidEye and statistical analyses), Edwin Raczko (LDA, NPMANOVA statistical analyses), Zbigniew Bochenek (plant traits), Andrzej Kłos (heavy metals), Anna Jarocińska (vegetation indices) analyzed the data, and Bogdan Zagajewski, Hans Tømmervik, Jarle W. Bjerke, Edwin Raczko, Zbigniew Bochenek, Andrzej Kłos, Anna Jarocińska, Samantha Lavender wrote the paper.

Conflicts of Interest: The authors declare no conflict of interest.

References

1. Jia, G.J.; Epstein, H.E.; Walker, D.A. Greening of arctic Alaska, 1981–2001. *Geophys. Res. Lett.* **2003**, *30*, 2067–2070. [CrossRef]
2. Beck, P.S.A.; Goetz, S.J. Satellite observations of high northern latitude vegetation productivity changes between 1982 and 2008: Ecological variability and regional differences. *Environ. Res. Lett.* **2011**, *6*, 045501. [CrossRef]
3. Xu, L.; Myneni, R.B.; Chapin, F.S., III; Callaghan, T.V.; Pinzon, J.E.; Tucker, C.J.; Zhu, Z.; Bi, J.; Ciais, P.; Tømmervik, H.; et al. Temperature and Vegetation Seasonality Diminishment over Northern Lands. *Nat. Clim. Chang.* **2013**, *3*, 581–586. [CrossRef]
4. Beck, P.S.A.; Goetz, S.J.; Mack, M.C.; Alexander, H.D.; Jin, Y.; Randerson, J.T.; Loranty, M.M. The impacts and implications of an intensifying fire regime on Alaskan boreal forest composition and albedo. *Glob. Chang. Biol.* **2011**, *17*, 2853–2866. [CrossRef]
5. McDowell, N.G.; Coops, N.C.; Beck, P.S.A.; Chambers, J.Q.; Gangodagamage, C.; Hicke, J.A.; Huang, C.; Kennedy, R.; Krofcheck, D.J.; Litvak, M.; et al. Global satellite monitoring of climate-induced vegetation disturbances. *Trends Plant Sci.* **2015**, *20*, 114–123. [CrossRef] [PubMed]
6. Bjerke, J.W.; Treharne, R.; Vikhamar-Schuler, D.; Karlsen, S.R.; Ravolainen, V.; Bokhorst, S.; Phoenix, G.K.; Bochenek, Z.; Tømmervik, H. Understanding the drivers of extensive plant damage in boreal and Arctic ecosystems: Insights from field surveys in the aftermath of damage. *Sci. Total Environ.* **2017**, *599–600*, 1965–1976. [CrossRef] [PubMed]
7. Bokhorst, S.F.; Bjerke, J.W.; Tømmervik, H.; Callaghan, T.V.; Phoenix, G.K. Winter warming events damage sub-Arctic vegetation: Consistent evidence from an experimental manipulation and a natural event. *J. Ecol.* **2009**, *97*, 1408–1415. [CrossRef]
8. Bjerke, J.W.; Karlsen, S.R.; Høgda, K.A.; Malnes, E.; Jepsen, J.U.; Lovibond, S.; Vikhamar Schuler, D.; Tømmervik, H. Record-low primary productivity and high plant damage in the Nordic Arctic Region in 2012 caused by multiple weather events and pest outbreaks. *Environ. Res. Lett.* **2014**, *9*, 084006. [CrossRef]
9. *Snow, Water, Ice and Permafrost in the Arctic (SWIPA): Climate Change and the Cryosphere*; Arctic Monitoring and Assessment Programme (AMAP): Oslo, Norway, 2011.
10. Tømmervik, H. Vegetation damage studies in the Jarfjordfjell area, Northern Norway, by use of airborne CASI spatial mode data. *Remote Sens. Rev.* **2000**, *18*, 19–51. [CrossRef]
11. Tømmervik, H.; Høgda, K.A.; Solheim, I. Monitoring vegetation changes in Pasvik (Norway) and Pechenga in Kola Peninsula (Russia) using multi-temporal Landsat MSS/TM data. *Remote Sens. Environ.* **2003**, *85*, 370–388. [CrossRef]
12. Askaer, L.; Schmidt, L.B.; Elberling, B.; Asmund, G.; Jonsdottir, I.S. Environmental impact on an Arctic Soil–Plant System resulting from metals released from coal mine waste in Svalbard (78° N). *Water Air Soil Pollut.* **2008**, *195*, 99–114. [CrossRef]
13. Thenkabail, P.S.; Smith, R.B.; De Pauw, E. Hyperspectral vegetation indices and their relationships with agricultural crop characteristics. *Remote Sens. Environ.* **2000**, *71*, 158–182. [CrossRef]

14. Kycko, M.; Zagajewski, B.; Kozlowska, A. Variability in spectral characteristics of trampled high-mountain grasslands. *Misc. Geogr.* **2014**, *18*, 10–14. [CrossRef]
15. Jarocińska, A.M.; Kacprzyk, M.; Marcinkowska-Ochtyra, A.; Ochtyra, A.; Zagajewski, B.; Meuleman, K. The application of APEX images in the assessment of the state of non-forest vegetation in the Karkonosze Mountains. *Misc. Geogr.* **2016**, *20*, 21–27. [CrossRef]
16. Solheim, I.; Engelsen, O.; Hosgood, B.; Andreoli, G. Measurement and Modeling of the Spectral and Directional Reflection Properties of Lichen and Moss Canopies. *Remote Sens. Environ.* **2000**, *72*, 78–94. [CrossRef]
17. Rees, W.G.; Tutubalina, O.V.; Golubeva, E.I. Reflectance spectra of subarctic lichens between 400 and 2400 nm. *Remote Sens. Environ.* **2004**, *90*, 281–292. [CrossRef]
18. Vierling, L.A.; Deering, D.W.; Eck, T.F. Differences in arctic tundra vegetation type and phenology as seen using bidirectional radiometry in the early growing season. *Remote Sens. Environ.* **1997**, *60*, 71–82. [CrossRef]
19. Buchhorn, M.; Walker, D.A.; Heim, B.; Raynolds, M.K.; Epstein, H.E.; Schwider, M. Ground-Based Hyperspectral Characterization of Alaska tundra vegetation along environmental gradients. *Remote Sens. Environ.* **2013**, *5*, 3971–4005. [CrossRef]
20. Adam, E.; Mutanga, O. Spectral discrimination of papyrus vegetation (*Cyperus papyrus* L.) in swamp wetlands using field spectrometry. *ISPRS J. Photogramm. Remote Sens.* **2009**, *64*, 612–620. [CrossRef]
21. Campioli, M.; Street, L.E.; Michelsen, A.; Shaver, G.R.; Maere, T.; Samson, R.; Lemeru, R. Determination of leaf area index, total foliar N, and normalized difference vegetation index for Arctic ecosystems dominated by *Cassiope tetragona*. *Arct. Antarct. Alp. Res.* **2009**, *4*, 426–433. [CrossRef]
22. Zagajewski, B. Assessment of neural networks and Imaging Spectroscopy for vegetation classification of the High Tatras. *Teledetekcja Środowiska* **2011**, *43*, 113.
23. Jelének, J.; Kupková, L.; Zagajewski, B.; Březina, S.; Ochytra, A.; Marcinkowska, A. Laboratory and image spectroscopy for evaluating the biophysical state of meadow vegetation in the Krkonoše National Park. *Misc. Geogr.* **2014**, *18*, 15–22. [CrossRef]
24. Marcinkowska, A.; Zagajewski, B.; Ochtyra, A.; Jarocińska, A.; Raczko, E.; Kupková, L.; Stych, P.; Meuleman, K. Mapping vegetation communities of the Karkonosze National Park using APEX hyperspectral data and Support Vector Machines. *Misc. Geogr.* **2014**, *18*, 23–29. [CrossRef]
25. Walker, D.A.; Raynolds, M.K.; Daniëls, F.J.A.; Einarsson, E.; Elvebakk, A.; Gould, W.A.; Katenin, A.E.; Kholod, S.S.; Markon, C.J.; Melnikov, E.S.; et al. The Circumpolar Arctic Vegetation Map. *J. Veg. Sci.* **2005**, *16*, 267–282. [CrossRef]
26. Epstein, H.E.; Raynolds, M.K.; Walker, D.A.; Bhatt, U.S.; Tucker, C.J.; Pinzon, J.E. Dynamics of aboveground phytomass of the circumpolar Arctic tundra during the past three decades. *Environ. Res. Lett.* **2012**, *7*, 015506. [CrossRef]
27. Johansen, B.E.; Karlsen, S.R.; Tømmervik, H. Vegetation mapping of Svalbard utilising Landsat TM/ETM+ data. *Polar Rec.* **2012**, *48*, 47–63. [CrossRef]
28. Johansen, B.E.; Tømmervik, H. The relationship between phytomass, NDVI and vegetation communities on Svalbard. *Int. J. Appl. Earth Obs. Geoinf.* **2013**, *27*, 20–30. [CrossRef]
29. Tømmervik, H.; Karlsen, S.R.; Nilsen, L.; Johansen, B.; Storvold, R.; Zmarz, A.; Beck, P.S.; Johansen, K.S.; Høgda, K.A.; Goetz, S.; et al. Use of unmanned aircraft systems (UAS) in a multiscale vegetation index study of Arctic plant communities in Adventdalen on Svalbard. *EARSeL eProceed.* **2014**, *13*, 47–52. [CrossRef]
30. Store Norske Spitsbergen Kullkompani AS. Available online: https://snl.no/Store_Norske_Spitsbergen_Kulkompani_AS (accessed on 30 December 2016).
31. Kłos, A.; Bochenek, Z.; Bjerke, J.W.; Zagajewski, B.; Ziółkowski, D.; Ziembik, Z.; Rajfur, M.; Dołhańczuk-Śródka, A.; Tømmervik, H.; Krems, P.; et al. The use of mosses in biomonitoring of selected areas in Poland and Spitsbergen in the years from 1975 to 2014. *Ecol. Chem. Engine* **2015**, *S22*, 201–218. [CrossRef]
32. Van der Wal, R.; Stien, A. High-arctic plants like it hot: A long-term investigation of between-year variability in plant biomass. *Ecology* **2014**, *95*, 3414–3427. [CrossRef]
33. Hansen, B.B.; Isaksen, K.; Benestad, R.E.; Kohler, J.; Pedersen, Å.Ø.; Loe, L.E.; Coulson, S.J.; Larsen, J.O.; Varpe, Ø. Warmer and wetter winters: Characteristics and implications of an extreme weather event in the High Arctic. *Environ. Res. Lett.* **2014**, *9*, 114021. [CrossRef]

34. Aarrestad, P.A.; Bakkestuen, V.; Hassel, K.; Stabbetorp, O.E.; Wilmann, B. *Establishment of Monitoring Sitres for Ground Vegetation in Endalen, Svalbard 2009*; NINA Report 579; Norsk Institutt for Naturforskning: Trondheim, Norway, 2010; pp. 1–62.
35. Hultén, E.; Fries, M. *Atlas of North European Vascular Plants: North of the Tropic of Cancer*; Koeltz Scientific Books: Königstein, Germany, 1986.
36. Mierczyk, M.; Zagajewski, B.; Jarocińska, A.; Knapik, R. Assessment of Imaging Spectroscopy for rock identification in the Karkonosze Mountains, Poland. *Misc. Geogr.* **2016**, *20*, 34–40. [CrossRef]
37. Lichtenthaler, H.K.; Buschmann, C.; Rinderle, U.; Schmuck, G. Application of chlorophyll fluorescence in ecophysiology. *Radiat. Environ. Biophys.* **1986**, *25*, 297–308. [CrossRef] [PubMed]
38. Clark, M.; Roberts, D.; Clark, D. Hyperspectral discrimination of tropical rain forest tree species at leaf to crown scales. *Remote Sens. Environ.* **2005**, *96*, 375–398. [CrossRef]
39. Anderson, M.J. A new method for non-parametric multivariate analysis of variance. *Austral Ecol.* **2001**, *26*, 32–46. [CrossRef]
40. Kłos, A.; Ziembik, Z.; Rajfur, M.; Dołhańczuk-Śródka, A.; Bochenek, Z.; Bjerke, J.W.; Tømmervik, H.; Zagajewski, B.; Ziółkowski, D.; Jerz, D.; et al. The Origin of Heavy Metals and Radionuclides Accumulated in the Soil and Biota Samples Collected in Svalbard, Near Longyearbyen. *Ecol. Chem. Eng. S* **2017**, *24*, 223–238. [CrossRef]
41. Kupková, L.; Červená, L.; Suchá, R.; Jakešová, L.; Zagajewski, B.; Březina, S.; Albrechtová, J. Classification of Tundra Vegetation in the Krkonoše Mts. National Park Using APEX, AISA Dual and Sentinel-2A Data. *Eur. J. Remote Sens.* **2017**, *50*, 29–46. [CrossRef]
42. Kycko, M.; Zagajewski, B.; Zwijacz-Kozica, M.; Cierniewski, J.; Romanowska, E.; Orłowska, K.; Ochtyra, A.; Jarocińska, A. Assessment of Hyperspectral Remote Sensing for Analyzing the Impact of Human Trampling on Alpine Swards. *Mt. Res. Dev.* **2017**, *37*, 66–74. [CrossRef]
43. Marcinkowska-Ochtyra, A.; Zagajewski, B.; Ochtyra, A.; Jarocińska, A.; Wojtuń, B.; Rogass, C.; Mielke, C.; Lavender, S. Subalpine and alpine vegetation classification based on hyperspectral APEX and simulated EnMAP images. *Int. J. Remote Sens.* **2017**, *38*, 1839–1864. [CrossRef]
44. Rouse, J.W.; Haas, R.H.; Schell, J.A.; Deering, D.W. Monitoring Vegetation Systems in the Great Plains with ERTS. In Proceedings of the 3rd Earth Resources Technology Satellite (ERTS) Symposium, Washington, DC, USA, 10–14 December 1973; NASA: Washington, DC, USA, 1973; pp. 309–317.
45. Bokhorst, S.F.; Phoenix, G.K.; Berg, M.P.; Callaghan, T.V.; Kirby-Lambert, C.; Bjerke, J.W. Climatic and biotic extreme events moderate long-term responses of above- and belowground sub-Arctic heathland communities to climate change. *Glob. Chang. Biol.* **2015**, *21*, 4063–4075. [CrossRef] [PubMed]
46. Olofsson, P.; Foody, G.M.; Stehman, S.V.; Woodcock, C.E. Making better use of accuracy data in land change studies: Estimating accuracy and area and quantifying uncertainty using stratified estimation. *Remote Sens. Environ.* **2013**, *129*, 122–131. [CrossRef]
47. Hunt, E.R., Jr.; Rock, B.N. Detection of changes in leaf water content using Near- and Middle-Infrared reflectances. *Remote Sens. Environ.* **1989**, *30*, 43–54. [CrossRef]
48. Birth, G.S.; McVey, G.R. Measuring the color of growing turf with a reflectance spectrophotometer. *Agron. J.* **1968**, *60*, 640–643. [CrossRef]
49. Huete, A.; Didan, K.; Miura, T.; Rodriguez, E.P.; Gao, X.; Ferreira, L. Overview of the Radiometric and Biophysical Performance of the MODIS Vegetation Indices. *Remote Sens. Environ.* **2002**, *83*, 195–213. [CrossRef]
50. Gitelson, A.A.; Merzlyak, M.N. Spectral Reflectance Changes Associated with Autumn Senescence of *Aesculus hippocastanum* L. and *Acer platanoides* L. Leaves. Spectral Features and Relation to Chlorophyll Estimation. *J. Plant Physiol.* **1994**, *143*, 286–292. [CrossRef]
51. Sims, D.A.; Gamon, J.A. Relationships between leaf pigment content and spectral reflectance across a wide range of species, leaf structures and developmental stages. *Remote Sens. Environ.* **2002**, *81*, 337–354. [CrossRef]
52. Anderson, H.B.; Nilsen, L.; Tømmervik, H.; Karlsen, S.R.; Nagai, S.; Cooper, E.J. Using Ordinary Digital Cameras in Place of Near-Infrared Sensors to Derive Vegetation Indices for Phenology Studies of High Arctic Vegetation. *Remote Sens.* **2016**, *8*, 847. [CrossRef]
53. Datt, B. A New Reflectance Index for Remote Sensing of Chlorophyll Content in Higher Plants: Tests Using Eucalyptus Leaves. *J. Plant Physiol.* **1999**, *154*, 30–36. [CrossRef]

54. Curran, P.J.; Windham, W.R.; Gholz, H.L. Exploring the relationship between reflectance red edge and chlorophyll concentration in slash pine leaves. *Tree Phys.* **1995**, *15*, 203–206. [CrossRef]
55. Guyot, G.; Baret, F. Utilisation de la haute resolution spectrale pour suivre l'etat des couverts vegetaux. In *ESA Special Publication, Proceedings of the 4th International Colloquium on Spectral Signatures of Objects in Remote Sensing, Paris, France, 18–22 January 1988*; European Space Agency: Paris, France, 1988; pp. 279–286.
56. Mascarini, L.; Lorenzo, G.A.; Vilella, F. Leaf Area Index, Water Index, and Red: Far Red Ratio Calculated by Spectral Reflectance and its Relation to Plant Architecture and Cut Rose Production. *J. Amer. Soc. Hort. Sci.* **2006**, *131*, 313–319.
57. Peng, D.; Zhang, X.; Zhang, B.; Liu, L.; Liu, X.; Huete, A.R.; Huang, W.; Wang, S.; Luo, S.; Zhang, X.; Zhang, H. Scaling effects on spring phenology detections from MODIS data at multiple spatial resolutions over the contiguous United States. *ISPRS J. Photogramm. Remote Sens.* **2017**, *132*, 185–198. [CrossRef]
58. Merzlyak, M.N.; Gitelson, A.A.; Chivkunova, O.B.; Rakitin, V.Y.U. Non-destructive Optical Detection of Pigment Changes during Leaf Senescence and Fruit Ripening. *Physiol. Plant.* **1999**, *106*, 135–141. [CrossRef]
59. Gitelson, A.A.; Zur, Y.; Chivkunova, O.B.; Merzlyak, M.N. Assessing Carotenoid Content in Plant Leaves with Reflectance Spectroscopy. *Photochem. Photobiol.* **2002**, *75*, 272–281. [CrossRef]
60. Gitelson, A.A.; Merzlyak, M.N.; Chivkunova, O.B. Optical Properties and Nondestructive Estimation of Anthocyanin Content in Plant Leaves. *Physiol. Plant.* **2001**, *71*, 38–45. [CrossRef]
61. R Core Team. *R: A Language and Environment for Statistical Computing*; R Foundation for Statistical Computing: Vienna, Austria, 2015.
62. Weihs, C.; Ligges, U.; Luebke, K.; Raabe, N. klaR Analyzing German Business Cycles. In *Data Analysis and Decision Support*; Baier, D., Decker, R., Schmidt-Thieme, L., Eds.; Springer: Berlin, Germany, 2005; pp. 335–343.
63. Venables, W.N.; Ripley, B.D. *Modern Applied Statistics with S*, 4th ed.; Springer: New York, NY, USA, 2002; ISBN 0-387-95457-0.
64. Community Ecology Package, Version 2.4-5. Available online: https://cran.r-project.org/web/packages/vegan/vegan.pdf (accessed on 11 December 2017).
65. Jones, T.G.; Coops, N.C.; Sharma, T. Employing Ground-Based Spectroscopy for Tree-Species Differentiation in the Gulf Islands National Park Reserve. *Int. J. Remote Sens.* **2010**, *31*, 1121–1127. [CrossRef]
66. Kycko, M. Assessment of the Dominant Alpine Sward Species Condition of the Tatra National Park Using Hyperespectral Remote Sensing. Ph.D. Thesis, Faculty of Geography and Regional Studies, University of Warsaw, Warsaw, Poland, 31 October 2017; pp. 279–286.
67. Roy, D.P.; Li, J.; Zhang, H.K.; Huang, H.; Li, Z. Examination of Sentinel-2A multi-spectral instrument (MSI) reflectance anisotropy and the suitability of a general method to normalize MSI reflectance to nadir BRDF adjusted reflectance. *Remote Sens. Environ.* **2017**, *199*, 25–38. [CrossRef]
68. Baret, F.; Jacquemond, S.; Leprieur, C.; Guyot, G. Are the spectral shifts an operational concept? Critical analysis of theoretical and experimental results. In Proceedings of the Second Airborne Visible/Infrared Imaging Spectrometer (AVIRIS) Workshop, Pasadena, CA, USA, 4–5 June 1990; Green, R.O., Ed.; 1990; pp. 58–71.
69. Zagajewski, B. Assessment of a possibility of the lead detection in grasses using spectrometer SPZ-5. In *A Decade of Trans-European Remote Sensing Cooperation, Proceedings of the 20th Annual Symposium of the European Association of Remote Sensing Laboratories (EARSeL), Dresden, Germany, 14–16 June 2000*; Buchroithner, M.F., Ed.; A.A. Balkema Publishers: Leiden, The Netherlands, 2001; pp. 367–371.